

Kelvin-Helmholtz billow evolution from a localized source

By W.D. Smyth^{1, *}

¹*College of Oceanic and Atmospheric Sciences, Oregon State University, USA*

SUMMARY

The envelope function for Kelvin-Helmholtz billows growing from a point disturbance is derived on the basis of linear perturbation theory. The result describes an elliptical patch of billows that expands linearly in time as the billows grow. An analytical model of the dispersion relation is used to derive quantitative expressions for the spreading rate and ellipticity of the patch as functions of the bulk Richardson number. The theoretical results are verified using a combination of two- and three-dimensional nonlinear simulations, and are compared with visual observations of billow patches in the atmosphere.

KEYWORDS: Billow Flow Instability Stratified shear flow Turbulence

1. INTRODUCTION

Banded clouds arising from Kelvin-Helmholtz (KH) instability typically occur in patches, extending over several wavelengths in the streamwise direction and a comparable (though generally unequal) distance in the cross-stream direction. Billow patches are readily observed in morning or early evening skies, and have been documented photographically by a number of investigators (*Ludlam, 1967; Thorpe, 2002*). KH billows have also been observed using various remote sensing methods (*e.g. Chapman and Browning, 1997, 1999*), and a similar phenomenon is common in the ocean thermocline (*e.g. Woods, 1968; Smyth et al., 2001*).

The most common theoretical description for billows employs unstable normal modes of a horizontally homogeneous, parallel, stratified shear layer. Given sufficiently strong shear, modes grow exponentially. Instabilities are seeded by small-amplitude, quasi-random disturbances, or “noise”, which is always present in natural flows. After many e-foldings, the disturbance is dominated by the fastest-growing mode, which has wavelength about seven times the depth of the shear layer.

The above scenario does not explain the fact that billows do not normally cover the entire sky, but rather are restricted to finite regions, or patches. One may imagine two possible explanations for this. One is that the conditions for instability (*e.g. strong shear*) exist only over a finite region, and it is in this region that billows grow. An alternative possibility is that the instability originates from a spatially localized disturbance and then spreads horizontally as it grows. In either case, the ultimate result is a field of billows having the wavelength of the fastest-growing mode and filling the region in which the ambient flow is unstable. At finite times, however, patch geometries resulting from these two scenarios may differ dramatically.

* Corresponding address: College of Oceanic and Atmospheric Sciences, Oregon State University, Corvallis OR, USA 97331, email: smyth@coas.oregonstate.edu

© Royal Meteorological Society, .

My objective here is to explore the second scenario, i.e., the growth of billows originating at a point source. The problem of instability growth from a point source is of interest for two main reasons. First, it represents the “impulse response” from which the response to any horizontally inhomogeneous noise distribution may be calculated. Second, it may in itself be a valid model for some geophysical events. Even in the stationary, homogeneous limit, turbulent flow features rare, intense disturbances that dominate the higher-order statistics (*Kolmogorov*, 1962; *Baker and Gibson*, 1987; *Frisch*, 1995). One can imagine that such events could serve as nucleation sites for KH instability. For example, *Thorpe* (2002) describes pairs of billow patches that overlap and merge as they grow. These might well represent the response to a pair of localized maxima in the ambient turbulence field. I will develop simple formulae that predict the impulse response at any level of shear and stratification, and thus permit assessment of the role that this mechanism plays in any geophysical regime where billows occur. In section 2, I use linear theory to make some simple predictions about the geometry of a billow patch evolving from a point source. These predictions are tested in section 3 using nonlinear numerical simulations. Conclusions are summarized in section 4.

2. THE LINEAR INITIAL VALUE PROBLEM

(a) General theory

The objective of this section is to develop a theory of billow growth from a point source based on a linear initial value problem. I assume that the perturbations are of infinitesimal amplitude, and that they can be represented as a superposition of temporally-growing normal modes. In general, the impulse response function can be written as

$$f(x, y, z, t) = \int_{-\infty}^{\infty} d\mu \hat{f}(z, \mu) F(x, y, t, \mu) + \text{c.c.}, \quad (1)$$

where

$$F(x, y, t, \mu) = \int_{-\infty}^{\infty} dk \int_{-\infty}^{\infty} dl \exp\{\sigma(k, l, \mu)t + i(kx + ly)\}. \quad (2)$$

The function f represents any perturbation quantity, σ is a (generally) complex growth rate, (k, l) is a real wave vector and “c.c.” denotes the complex conjugate. The coordinates x , y and z denote the streamwise, spanwise and vertical directions respectively, and t is the time. The parameter μ enumerates a complete set of vertical structure functions \hat{f} , including both the continuous spectrum of neutral modes and the discrete spectrum of growing and decaying modes. Here, I will focus on the (x, y, t) dependence of the impulse response function, as expressed in F . In addition, I will assume that the response of an unstable flow is dominated by a single value of μ that represents the fastest growing mode for any wave vector (k, l) , and hence rewrite (2) in the more compact form

$$F(x, y, t) = \int_{-\infty}^{\infty} dk \int_{-\infty}^{\infty} dl \exp\{\sigma(k, l)t + i(kx + ly)\}. \quad (3)$$

Note that this assumption excludes the possibility of nonmodal growth. The validity of the assumptions embodied in (3), and others yet to arise, will be tested by means of numerical solutions of the initial value problem.

The modal parameters σ , k and l obey a dispersion relation whose form must be established before (3) can be evaluated. I will assume that the flow is inviscid, nondiffusive and Boussinesq, and that background profiles of streamwise velocity $U(z)$ and buoyancy frequency $N(z)$ are given. In this case, the dispersion relation can be written as

$$\sigma = \sigma(k, l; U(z), N(z)). \quad (4)$$

The problem is now nondimensionalized by defining a length scale h_0 , a velocity scale Δu and a density scale $\Delta \rho$, such that the background profiles can be expressed as

$$U = g_1(z); \quad N^2 = Jg_2(z), \quad (5)$$

where g_1 and g_2 are nondimensional functions of the nondimensional height z such that

$$\max_z |dg_1/dz| = \max_z |g_2| = 1 \quad (6)$$

and $J = g\Delta\rho h_0/\rho_0\Delta u^2$ is a bulk Richardson number. The constants g and ρ_0 represent the gravitational acceleration and a characteristic value for the density. With fixed definitions for g_1 and g_2 , the dispersion relation now collapses to

$$\sigma = \sigma(k, l, J). \quad (7)$$

Normal modes with $k \neq 0$; $l = 0$, i.e. with wave vector aligned with the background flow $U(z)$, will be referred to as *two-dimensional* because they do not depend on the y coordinate. Modes with $l \neq 0$ are called *oblique*. The angle of obliquity, θ , is defined by $\cos \theta = k/\tilde{k}$, where $\tilde{k} = \sqrt{k^2 + l^2}$ is the magnitude of the wave vector.

In the theory to follow, σ will be expanded in a truncated Taylor series about a wavenumber at which σ_r (where the subscript indicates the real part) is a local maximum. I will assume that this wavenumber lies on the k axis, i.e. that the fastest-growing mode is two-dimensional. In preparation for this procedure, I now describe some general properties of the dispersion relation (7). The extension of Squire's theorem due to *Yih* (1955) shows that an oblique mode feels only the component of the background shear parallel to its own wave vector. Hence

$$\sigma(k, l, J) = \cos \theta \cdot S(\tilde{k}, \tilde{J}), \quad (8)$$

where

$$S(k, J) = \sigma(k, 0, J) \quad (9)$$

is the dispersion relation for two-dimensional modes and $\tilde{J} = J/\cos^2 \theta$ is the equivalent bulk Richardson number. Note that $\cos \theta$, \tilde{k} and \tilde{J} are all even functions of l , and therefore so is σ . As a result,

$$\left. \frac{\partial \sigma}{\partial l} \right|_{l=0} = 0. \quad (10)$$

Since this result holds for all k , we also have

$$\left. \frac{\partial^2 \sigma}{\partial k \partial l} \right|_{l=0} = 0. \quad (11)$$

Moreover, it may be shown that

$$\left. \frac{\partial^2 \sigma}{\partial l^2} \right|_{l=0} = \frac{1}{k} \frac{\partial S}{\partial k} + \frac{2J^{3/2}}{k^2} \frac{\partial}{\partial J} \left(\frac{S}{J^{1/2}} \right). \quad (12)$$

Taking the real part and evaluating at $k = k_0$ such that

$$\frac{\partial S_r}{\partial k} = 0, \quad (13)$$

one obtains

$$\left. \frac{\partial^2 \sigma_r}{\partial l^2} \right|_{k=k_0, l=0} = \frac{2J^{3/2}}{k^2} \frac{\partial}{\partial J} \left(\frac{S_r}{J^{1/2}} \right) \Big|_{k=k_0, l=0}. \quad (14)$$

This result is true for any inviscid, nondiffusive, parallel shear flow. It tells us that a two-dimensional mode can represent at least a local maximum in the growth rate (with respect to k and l) as long as the growth rate does not increase with increasing stratification any faster than $J^{1/2}$. Conversely, if growth rate increases with J faster than $J^{1/2}$, the fastest-growing mode must be oblique.

Stratified shear flows for which the fastest-growing mode is oblique have been described by *Smyth* (1990) and *Smyth and Moum* (2002); however, these flows exist only in a very limited region of parameter space. For most mean flows that yield KH-like instabilities, including the model to be used here, the fastest-growing instability is two-dimensional.

I now construct a second order Taylor series expansion of σ about a point $k = k_0, l = 0$ where the growth rate is a maximum. Anticipating the application to KH instability, I assume that the unstable modes of interest are stationary, i.e. that their growth rates are purely real. (Incorporation of oscillatory modes is interesting, but it adds complication and is unnecessary here.) The expansion therefore reads

$$\sigma(k, l, J) \approx \sigma_0(J) + \frac{1}{2} \sigma_{kk} (k - k_0)^2 + \frac{1}{2} \sigma_{ll} l^2. \quad (15)$$

Here, $\sigma_0(J)$ is the (real) maximum growth rate for a given J and $(k_0, 0)$ is the corresponding wave vector. The constants σ_{kk} and σ_{ll} are defined by

$$\sigma_{kk}(J) = - \left. \frac{\partial^2 \sigma_r}{\partial k^2} \right|_{k=k_0, l=0}; \quad \sigma_{ll}(J) = - \left. \frac{\partial^2 \sigma_r}{\partial l^2} \right|_{k=k_0, l=0}. \quad (16)$$

$F(x, y, t)$ may now be approximated using Laplace's method. Substituting (15) into (3) and integrating, one obtains

$$F(x, y, t) = \frac{2\pi}{\sqrt{\sigma_{kk}\sigma_{ll}t}} \exp \left\{ \sigma_0 t - \frac{x^2}{2\sigma_{kk}t} - \frac{y^2}{2\sigma_{ll}t} + ik_0 x \right\}. \quad (17)$$

Equation (17) describes a two-dimensional wave with wavenumber k_0 modulated by an elliptical envelope, i.e.:

$$F(x, y, t) = F_e(x, y, t) \exp(ik_0x), \quad (18)$$

in which

$$F_e(x, y, t) = \frac{2\pi}{\sqrt{\sigma_{kk}\sigma_{ll}t}} \exp\left\{\sigma_0t - \frac{x^2}{2\sigma_{kk}t} - \frac{y^2}{2\sigma_{ll}t}\right\}. \quad (19)$$

$F_e = \text{constant}$ describes a family of ellipses given by

$$x^2 + \frac{y^2}{R^2} = x_0^2. \quad (20)$$

$R = \sqrt{\sigma_{ll}/\sigma_{kk}}$ is the aspect ratio (cross-stream/streamwise) and is independent of time. The semi-major axis of each ellipse is given by

$$x_0(t) = \sqrt{2\sigma_{kk}t\left(\sigma_0t + \ln \frac{2\pi}{\sqrt{\sigma_{kk}\sigma_{ll}t}} - \ln F_e^C\right)}, \quad (21)$$

where F_e^C is the (constant) value of F_e that labels the ellipse. In the long-time limit, the first term in the parentheses dominates, hence both the major and minor axes grow linearly in time.

It is useful to have a definition for the ‘‘boundary’’ of the elliptical envelope, although that definition is necessarily arbitrary. Here, I will define the boundary as follows. The value of F_e at the spatial origin [given by (19) with $x = y = 0$] approaches positive infinity when $t = 0$, decreases to a minimum after one e-folding of the fastest-growing mode, and increases thereafter. The minimum value is $2\pi\sigma_0e/\sqrt{\sigma_{kk}\sigma_{ll}}$. The patch boundary will be defined as that member of the family of ellipses (20) upon which F_e takes this value. At very early times, the envelope shrinks, reaching zero size at $t = 1/\sigma_0$. After this time, the envelope expands monotonically in time. The semi-major axis of the envelope is given by

$$x_0(t) = \sqrt{2\sigma_{kk}t(\sigma_0t - \ln \sigma_0t - 1)} \quad (22)$$

for $\sigma_0t \geq 1$.

(b) Results for a model dispersion relation

To obtain more quantitative information, one must specify a form for the dispersion relation $S(k, J)$. For this purpose, I use the *ad hoc* model

$$S(k, J) = 4S_0(\sqrt{1/4 - J} + k - 1/2)(\sqrt{1/4 - J} - k + 1/2). \quad (23)$$

This model is based on the numerical stability analysis of the hyperbolic tangent shear layer

$$g_1 = \tanh z; \quad g_2 = \text{sech}^2 z \quad (24)$$

by *Hazel* (1972). The constant $S_0 = 0.19$ is Hazel's maximum growth rate for the case $J = 0$. The fastest-growing mode occurs at $k = 1/2$ for all J , which is within 10% of Hazel's result, and the stability boundary $J = k(1 - k)$ for (24) is reproduced exactly. The maximum growth rate decreases linearly from S_0 at $J = 0$ to zero at $J = 1/4$. While correct at the endpoints, this linear relation underestimates Hazel's growth rate by up to 10% for moderate J . The validity of this model will be tested in section 3 by means of numerical simulations of the nonlinear initial value problem.

Substituting (23) into (16) yields

$$\sigma_{kk} = 8S_0; \quad \sigma_{ll} = 4S_0(1 + 4J), \quad (25)$$

or

$$\sigma_{kk} = 8\sigma_0(J)/(1 - 4J); \quad \sigma_{ll} = 4\sigma_0(J)(1 + 4J)/(1 - 4J) \quad (26)$$

(recall that $\sigma_0(J)$ is the maximum growth rate for a given J). The semi-major axis of the envelope is therefore

$$x_0 = \frac{4\sigma_0 t}{\sqrt{1 - 4J}} \sqrt{1 - \frac{1 + \ln \sigma_0 t}{\sigma_0 t}}. \quad (27)$$

The streamwise/spanwise aspect ratio is given by

$$R = \sqrt{\frac{1 + 4J}{2}}, \quad (28)$$

which ranges from 0.71 in the unstratified limit to unity at $J = 1/4$. This model therefore implies that marginally unstable billow patches (J near $1/4$) will be nearly circular, while more strongly unstable patches will be elongated by up to $\sim 40\%$ in the streamwise direction. Visual observation of clouds often reveals elliptical billow patches with aspect ratios in this range.

Another easily observed property of billow patches in the atmosphere is the number of billows in the patch. This number is generally greater than two (so that the banded clouds may be recognized as such) but rarely exceeds ten. For comparison, I now give the corresponding result based upon the present theory. The nondimensional wavelength of the fastest-growing mode is given by $2\pi/k_0 = 4\pi$, and therefore the major axis of the ellipse, measured in wavelengths, is $2x_0/4\pi$ (Fig. 1). Once the envelope is growing linearly in time, it expands to cover an additional $2/\pi\sqrt{1 - 4J}$ billows with each e-folding of the dominant instability. This number ranges from 0.64 in the unstratified limit, to unity at $J = 0.15$, to $+\infty$ at the stability boundary $J = 0.25$. One normally expects that growth to observable amplitude will require "a few" e-folding times, e.g. a perturbation of scale 1m grows into a 100m-high billow in $\ln(100) = 4.6$ e-foldings. For J values between 0 and 0.20 (low enough to yield significant growth), 4.6 e-foldings is predicted to yield between 3 and 7 wavelengths, consistent with observations.

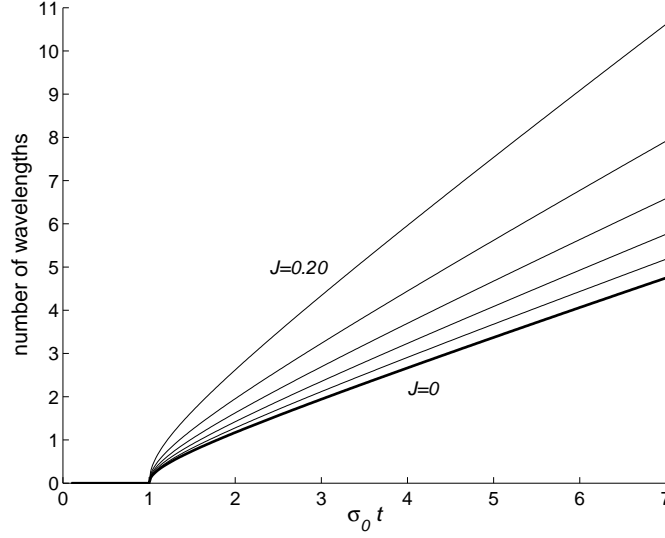


Figure 1. (a) Semi-major axis of the patch boundary (in wavelengths of the fastest-growing mode) as a function of time (in e-folding times of the fastest growing mode). The thick curve is for $J = 0$; successively higher curves are for $J = 0.04, 0.08, 0.12, 0.16$ and 0.20 , respectively.

(c) *The two-dimensional case*

In the next section, the theory developed here will be tested using nonlinear numerical simulations. These tests will be done in two dimensions as well as three, as the computational efficiency of the two-dimensional model allows exploration of a fuller range of ambient flow conditions. Although the process of billow growth from a point source is intrinsically three dimensional, the two dimensional model embodies most of the assumptions made in this section.

For the two-dimensional case, l is set to zero and the integration over l is omitted from (3). The envelope function is then given by

$$F_e^{2d}(x, t) = \sqrt{\frac{2\pi}{\sigma_{kk}t}} \exp \left\{ \sigma_0 t - \frac{x^2}{2\sigma_{kk}t} \right\}. \quad (29)$$

As in the three-dimensional case, the value of F_e^{2d} at the spatial origin decreases to a minimum, then increases. The minimum value now occurs after one half e-folding time of the dominant mode, and is equal to $\sqrt{4\pi\sigma_0 e/\sigma_{kk}}$. The “envelope” is now the one-dimensional interval $-x_0^{2d} \leq x \leq x_0^{2d}$, where

$$x_0^{2d}(t) = \sqrt{2\sigma_{kk}t \left(\sigma_0 t - \frac{1}{2} \ln 2\sigma_0 t - \frac{1}{2} \right)} \quad (30)$$

for $\sigma_0 t \geq 1/2$. For the dispersion relation (23), $\sigma_{kk} = 8S_0$ just as in the three-dimensional case, so that

$$x_0^{2d} = \frac{4\sigma_0 t}{\sqrt{1-4J}} \sqrt{1 - \frac{1 + \ln 2\sigma_0 t}{2\sigma_0 t}}. \quad (31)$$

In the long-time limit, x_0^{2d} evolves exactly as does $x_0(t)$ in the three-dimensional case.

3. NONLINEAR EVOLUTION

In this section, I test the results derived in section 2 using both two- and three-dimensional nonlinear simulations. Both models solve the Boussinesq equations in a domain with free-slip, insulating boundaries at top and bottom and periodic boundary conditions in the horizontal direction(s). Planetary rotation was neglected, since the time scale for billow evolution is normally much smaller than an inertial period. For consistency with the assumptions of section 2, hyperviscosity was used to damp the turbulent cascade at the smallest scales while leaving the mean flow and large eddies essentially inviscid. Flows were initialized using (24) plus a point disturbance at the domain center. In one instance, the hyperbolic secant stratification profile in (24) was replaced by uniform stratification, $N^2(z) = J$. Further details on the model runs may be found in the appendix and in table 1.

(a) Results from two-dimensional simulations

This subsection describes results from five two-dimensional simulations. Four were initialized with $J = 0.08, 0.12, 0.16$ and 0.20 . The fifth employed uniform stratification $N^2 = J$, with $J = 0.12$.

Figure 2 shows an illustrative example: snapshots of the density field from the $J = 0.12$ case. The disturbance was initiated at the domain center and quickly formed a pair of KH billows (Fig.2a). The patch grew over time via the appearance of new billows at its edges. The wavelengths of the billows did not change appreciably as they grew, and corresponded to the wavelength of the fastest-growing KH mode.

The largest inner billows ultimately paired. This subharmonic instability was more energetic in the $J = 0.08$ case, less so at $J = 0.16$ and did not occur at all at $J = 0.20$, as expected on the basis of linear theory (*Klaassen and Peltier, 1989*). The exponential growth described by (29) was arrested as the billows reached large amplitude. From that point on, the billows grew only by means of pairing.

Despite the manifest nonlinearity of the inner billows, the growth of the small billows at the patch edges, and hence of the patch itself, conformed very closely to the theory (Fig.3). In every case, a brief adjustment period was followed by linear spreading. The spreading rate compared remarkably well with the theory over the entire range of Richardson numbers.

The close correspondence with theory evident in Fig. 3 confirms the validity of the assumptions developed in section 2. It pertains, however, to only a single model for the shear layers that drive KH instability in the atmosphere and oceans. The correspondence is to some degree unsurprising because the theory rests in part upon the model dispersion relation (23), which is based closely on the stability characteristics of the particular profiles used to initialize the simulations.

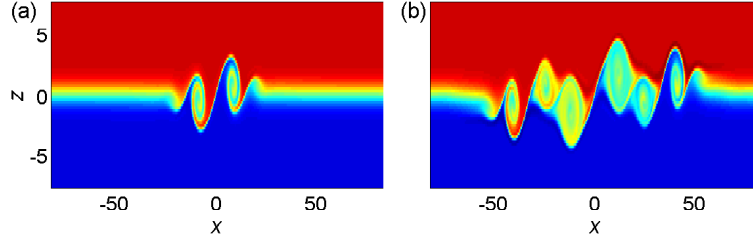


Figure 2. Density field from two-dimensional nonlinear simulation with $J = 0.12$. Values range from -1 (red) to +1 (blue). The vertical scale is exaggerated.

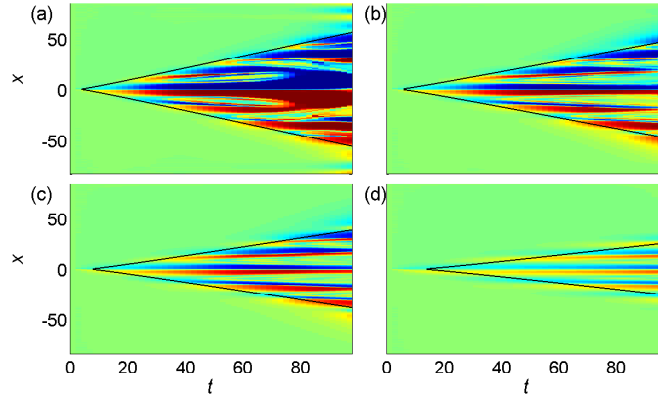


Figure 3. Hovmuller diagrams of midlevel ($z = 0$) density, from two-dimensional simulations with (a) $J = 0.08$, (b) $J = 0.12$, (c) $J = 0.16$ and (d) $J = 0.20$ (simulations 1-4 on table 1). Curves indicate envelope limits as defined in (31). Density values range from 1 (blue) to -1 (red).

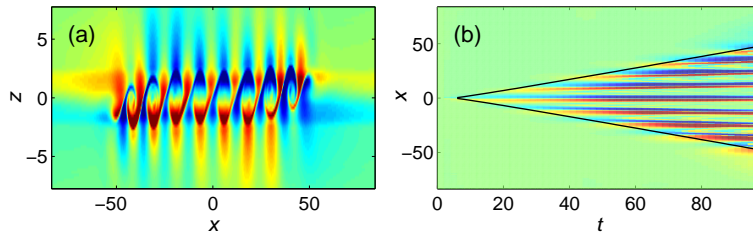


Figure 4. (a) Perturbation density field at $t = 100$ from two-dimensional simulation with uniform stratification ($J = 0.12$). (b) Hovmuller diagram of the midlevel density field from the same simulation. Curves indicate envelope limits as defined in (31). Density values range from 1 (blue) to -1 (red).

To test the validity of the theory for the more general class of stratified shear flows that may drive KH instability in nature, I conducted a fifth two-dimensional simulation, using as its initial condition a shear layer in a uniformly stratified fluid. This flow differs from the previous model largely in the potential for energy to radiate vertically in the form of gravity waves.

Figure 4a shows a representative snapshot of the perturbation density field. (The horizontal mean is subtracted off because its large variation across the domain tends to obscure the features of interest.) Most of the vertical radiation is in the form of evanescent waves (as seen by the lack of tilt) having the horizontal wavelength of the primary KH billows. Larger scale fluctuations are also evident, though, and these might well propagate far away from the shear layer in a model designed to accommodate that process. It is beyond the scope of this paper to investigate radiating modes in detail, but clearly the possibility exists for KH instability to amplify a point disturbance into a large-scale wave packet capable of generating envelope radiation (*Fritts, 1984; Scinocca and Ford, 2000*).

The main result of this comparison is shown in Fig. 4b. Despite the dramatic difference in ambient stratification, the spreading of the billow patch proceeds very similarly to the previous case with $J = 0.12$ (Fig.3b), and is therefore well described by the theory.

(b) *Results from three-dimensional simulations*

While two-dimensional simulations embody much of the physics of instability growth from a point source, they do not include the important contribution of oblique modes, as described in the previous section. That deficiency is now remedied via a pair of three-dimensional simulations. Aside from dimensionality, these simulations are virtually identical to the $J = 0.08$ and $J = 0.16$ cases of the previous subsection.

Instantaneous density fields from the $J = 0.08$ case are shown in Fig.5. The upper frame shows a sequence of approximately two-dimensional billows whose amplitude tapers off monotonically in the cross-stream direction. The anticipated dominance of two-dimensional unstable modes is confirmed by the absence of oscillations in y . However, the finite cross-stream extent of the patch indicates the important role played by oblique modes. The lower frame shows a later phase in the patch evolution, just before the front and rear boundaries encountered the ends of the periodic domain. The billow cores are now visibly turbulent. Striations in the y direction indicate secondary instability, and there is a suggestion of the localized pairing phenomenon described by *Thorpe (2002)*. This appears to be an expression of the broadband nature of the pairing instability (*Pierrehumbert, 1982; Smyth, 1994*), just as the patch envelope expresses the broadband nature of the primary instability.

The Hovmuller diagrams in Figs. 6a and c show that the streamwise extent of the patch increases in accordance with (22). Figures 6b and d contain snapshots of the density field along the central plane $z = 0$, illustrating the $x - y$ dependence of each billow patch. In each case, the aspect ratio of the patch is as predicted by (28). This provides striking confirmation of the validity of linear theory in describing the expansion of the patch, despite the highly nonlinear nature of the innermost billows.

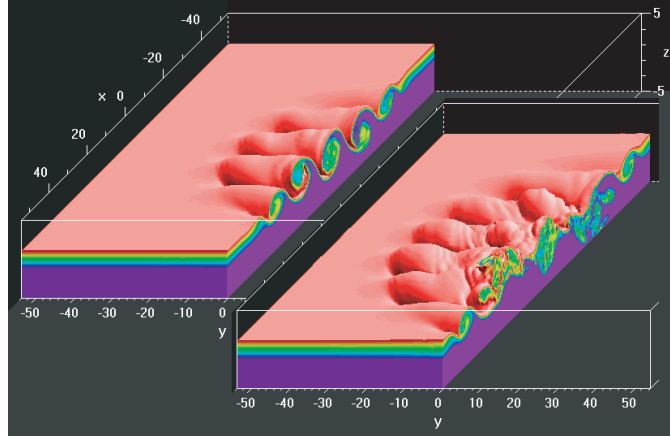


Figure 5. Density field from three-dimensional nonlinear simulation with $J = 0.08$ at times $t = 85$ (upper left) and $t = 103$ (lower right). Values range from 1 (blue) to -1 (red). Selected areas have been rendered transparent to expose the three-dimensional flow structure.

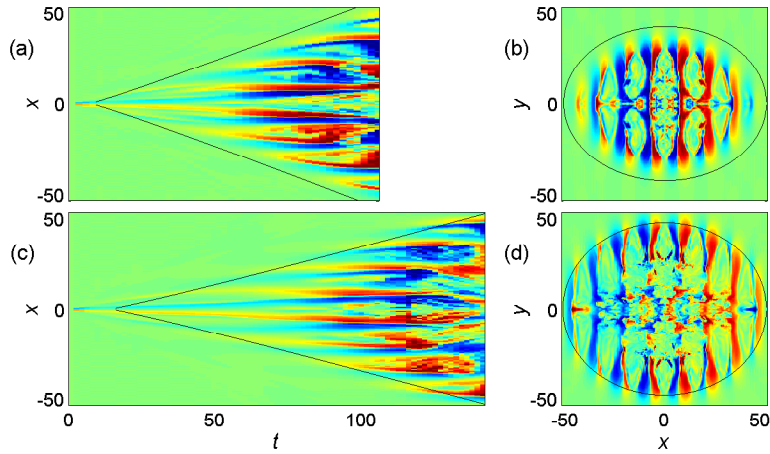


Figure 6. (a,c): Hovmuller diagrams for density field at $y = 0$, $z = 0$, from three-dimensional simulations with (a) $J = 0.08$ and (c) $J = 0.16$. Curves indicate envelope limits as defined in (22). (b,d): Instantaneous cross-sections of the density field at $z = 0$, from three-dimensional simulations with (b) $J = 0.08$, $t = 99$ and (d) $J = 0.16$, $t = 142$. Curves indicate the elliptical boundary defined by (20), with x_0 as defined in (22). In (c) and (d), only part of the horizontal domain is shown.

4. CONCLUSIONS

An analytical model has been developed to describe the spreading of KH billows seeded by a point disturbance. The theory embodies the following key assumptions:

1. Billow evolution is driven entirely by unstable normal modes, i.e. nonmodal growth is neglected.

2. Unstable modes are assumed to be (a) two-dimensional and (b) stationary with respect to the center of the shear layer.
3. The vertical dependence of the normal modes is neglected.
4. The integral over unstable modes is approximated using Laplace's method.
5. An *ad hoc* analytical model for the dispersion relation based on that for the hyperbolic tangent shear layer is adopted.

These assumptions have been validated by comparing the patch evolution that they imply with results from nonlinear simulations of the initial value problem. The spreading rate and the aspect ratio of the patch boundary, as well as the dependence of those parameters on the bulk Richardson number, are predicted very closely.

The main predictions of the theory are as follows:

1. Instability growing from a point source generates an elliptical patch of waves having the periodicity of the fastest-growing unstable mode.
2. After a brief adjustment period, the horizontal dimensions of the patch boundary increase linearly in time.
3. The aspect ratio of the ellipse remains constant as the patch expands. In conditions of strong stratification (with J only slightly less than $1/4$), patches are nearly circular. In the limit of weak stratification (strong instability), patches are elongated by a factor of $\sqrt{2}$ in the streamwise direction (Eq. 28).
4. Patches grow fastest in strongly unstable (high shear, low J) conditions. However, the ratio of the expansion rate to the growth rate of the billows is greatest when J is large. As a result, at a given stage of billow growth, a strongly stratified patch will contain more billows than a weakly stratified one (Eq. 27).

Patches arising from a point source as described here have much in common with those observed in nature. Any billow patch exhibiting an elliptical envelope may have grown from a localized disturbance; see Fig. 8 of *Ludlam* (1967) for a clear example. Of course, every billow patch is eventually constrained by the extent of the unstable region, which is in turn determined by whatever large-scale process drives the shear. For example, Fig. 16 of *Ludlam* (1967) shows a train of billows having aspect ratio far in excess of the maximum predicted here. The present results therefore indicate that that patch was constrained by inhomogeneity in the ambient flow, at least at the time the photograph was taken.

To summarize, instability growth from a point disturbance is an interesting and perhaps not entirely unrealistic model for billow patches in the atmosphere and oceans. Relaxation of assumptions 2a and 2b listed above would permit application of this theory to a wider range of background flow profiles such as stratified jets (.g. Sutherland and Peltier, 1992). Other issues meriting further investigation include the potential for gravity wave radiation and the effects of finite patch extent on the processes leading to turbulence.

ACKNOWLEDGEMENTS

I am indebted to Kraig Winters for the three-dimensional numerical code and to Steve Thorpe for helpful advice. This work was supported by the National Science Foundation under grant OCE0095640.

APPENDIX A

The numerical models

In this appendix I give brief descriptions of the numerical codes used in section 3. Further details on the two- and three-dimensional models may be found in *Smyth and Moum* (2002) and *Winters et al.* (2003), respectively.

Both nonlinear models of the initial value problem solve the field equations for incompressible flow in the Boussinesq limit:

$$\begin{aligned} \frac{\partial u_i}{\partial t} &= -u_j \frac{\partial u_i}{\partial x_j} - \frac{1}{\rho_0} \frac{\partial p}{\partial x_i} - J \frac{\rho - \rho_0}{\rho_0} \delta_{i3} + \frac{1}{Re_h} \nabla^4 u_i \\ \frac{\partial \rho}{\partial t} &= -u_j \frac{\partial \rho}{\partial x_j} + \frac{1}{Re_h} \nabla^4 \rho \\ \frac{\partial u_j}{\partial x_j} &= 0 \end{aligned} \tag{A.1}$$

The equations have been nondimensionalized as described in section 2. The vector u_i contains the components of the velocity field and ρ and p represent density and pressure, respectively. Hyperviscosity is used to control small-scale fluctuations while approximating the inviscid limit in the large scales. The parameter Re_h is chosen so that the smallest resolved scales are damped at a rate equivalent to Laplacian diffusion with coefficient $1/Re = 1/300$. ($Re = h_0 \Delta u / \nu$ is the Reynolds number and ν is the kinematic viscosity.) Both models impose free-slip, insulating conditions at the top and bottom, and periodic boundary conditions in the horizontal directions. Each simulation is terminated when the patch begins to interact with its periodic images (e.g. Fig. 3a).

Both codes use Fourier pseudospectral discretization in the horizontal. The three-dimensional code uses the same discretization in the vertical, while the two-dimensional code computes vertical derivatives using a fourth-order compact scheme (*Lele*, 1992).

Time stepping is via the third-order Adams-Bashforth method, with timestep determined by a Courant-Friedrichs-Lewy stability condition.

In all cases, the initial streamwise velocity profile was given by $g_1 = \tanh z$. The corresponding vorticity has a maximum value +1 on the plane $z = 0$. To simulate the effect of a point disturbance, the sign of that vorticity was simply reversed at the single point $x = y = z = 0$.

Additional details of the simulations are given in table 1. For the two-dimensional cases, a sequence of runs with initial stratification function $g_2 = \tanh z$ and increasing values of J revealed the influence of the bulk Richardson number on billow evolution. This sequence was followed by a fifth run with uniform initial stratification. For that case, absorbing layers were placed over the upper and lower 1/8 of the domain as described by *Smyth and Moum* (2002). The domain length was chosen to equal 12 wavelengths of the most unstable KH mode. For the three-dimensional simulations, the domain height was halved for economy, as the two-dimensional cases had shown that the larger height was not needed except in the case of uniform stratification. The horizontal domain dimensions were set equal. For the $J = 0.08$ case, the domain length was reduced to 8 wavelengths of the fastest-growing mode. In the $J = 0.16$ case, the domain length was restored to 12 wavelengths because the patch boundary was predicted (correctly) to contain more wavelengths at higher J .

REFERENCES

- | | | |
|-----------------------------------|------|---|
| Baker, M. and Gibson, C. | 1987 | Sampling turbulence in the stratified ocean: Statistical consequences of strong intermittency. <i>J. Phys. Oceanogr.</i> , 17 , 1817–1837 |
| Chapman, D. and Browning, K. | 1997 | Radar observation of wind shear splitting within evolving atmospheric Kelvin-Helmholtz billows. <i>Q. J. R. Meteorol. Soc.</i> , 107 , 351–365 |
| Chapman, D. and Browning, K. | 1999 | Release of potential shearing instability in warm frontal zones. <i>Q. J. R. Meteorol. Soc.</i> , 125 , 2265–2289 |
| Frisch, U. | 1995 | <i>Turbulence: The Legacy of A.N. Kolmogorov</i> . Cambridge University Press, Cambridge |
| Fritts, D. | 1984 | Shear excitation of atmospheric gravity waves. Part ii: Nonlinear radiation from a free shear layer. <i>J. Atmos. Sci.</i> , 41 (4), 524–537 |
| Hazel, P. | 1972 | Numerical studies of the stability of inviscid parallel shear flows. <i>J. Fluid Mech.</i> , 51 , 39–62 |
| Klaassen, G. and Peltier, W. | 1989 | The role of transverse secondary instabilities in the evolution of free shear layers. <i>J. Fluid Mech.</i> , 202 , 367–402 |
| Kolmogorov, A. | 1962 | A refinement of previous hypotheses concerning the local structure of turbulence in a viscous incompressible fluid at high Reynolds number. <i>J. Fluid Mech.</i> , 13 , 82–85 |
| Lele, S. | 1992 | Compact finite difference schemes with spectral-like resolution. <i>J. Comput. Phys.</i> , 103 , 16–42 |
| Ludlam, F. | 1967 | Characteristics of billow clouds and their relation to clear air turbulence. <i>Q. J. R. Meteorol. Soc.</i> , 93 , 419–435 |
| Pierrehumbert, R. and Widnall, S. | 1982 | The two- and three-dimensional instabilities of a spatially periodic shear layer. <i>J. Fluid Mech.</i> , 114 , 59–82 |
| Scinocca, J. and Ford, R. | 2000 | The nonlinear forcing of large-scale internal gravity waves by stratified shear instability. <i>J. Atmos. Sci.</i> , 57 , 653–672 |
| Smyth, W. and Moum, J. | 2002 | Shear instability and gravity wave saturation in an asymmetrically stratified jet. <i>Dyn. Atmos. Oceans</i> , 35 , 265–294 |

Smyth, W., Moum, J. and Caldwell, D.	2001	The efficiency of mixing in turbulent patches: inferences from direct simulations and microstructure observations. <i>J. Phys. Oceanogr.</i> , 31 , 1969–1992
Smyth, W. and Peltier, W.	1990	Three-dimensional primary instabilities of a stratified, dissipative, parallel flow. <i>Geophys. Astrophys. Fluid Dyn.</i> , 52 , 249–261
Smyth, W. and Peltier, W.	1994	Three-dimensionalization of barotropic vortices on the f-plane. <i>J. Fluid Mech.</i> , 265 , 25–64
Sutherland, B. and Peltier, W.	1992	The stability of stratified jets. <i>Geophys. Astrophys. Fluid Dyn.</i> , 66 , 101–131
Thorpe, S.	2002	The axial coherence of Kelvin-Helmholtz billows. <i>Q. J. R. Meteorol. Soc.</i> , 128 , 1529–1542
Winters, K., MacKinnon, J. and Mills, B.	2003	A spectral model for process studies of rotating, density-stratified flows. <i>J. Atmos. Oceanic Technol.</i> , 21 (1), 69–94
Woods, J.	1968	Wave-induced shear instability in the summer thermocline. <i>J. Fluid Mech.</i> , 32 , 791–800
Yih, C.-S.	1955	Stability of two-dimensional parallel flows for three-dimensional disturbances. <i>Quart. Appl. Math.</i> , 12 , 434–435

Simulation	J	g_2	L_x	L_y	L_z	N_x	N_y	N_z
1	0.08	$\tanh z$	160	0	21	384	0	96
2	0.12	$\tanh z$	160	0	21	384	0	96
3	0.16	$\tanh z$	160	0	21	384	0	96
4	0.20	$\tanh z$	160	0	21	384	0	96
5	0.12	1	160	0	21	384	0	96
6	0.08	$\tanh z$	107	107	10	256	256	24
7	0.16	$\tanh z$	160	160	10	256	256	24

TABLE A.1. Parameters for numerical simulations. J and g_2 are the bulk Richardson number and stratification function, such that the initial profile of the squared buoyancy frequency is $N^2 = Jg_2(z)$. The corresponding initial velocity profile is $g_1 = \tanh z$ in all cases. L_x , L_y and L_z are the domain dimensions in the streamwise, cross-stream and vertical directions, respectively, and N_x , N_y and N_z are the corresponding array sizes.